Alexandria Engineering Journal (2021) 60, 2885–2903

HOSTED BY

Alexandria University

Alexandria Engineering Journal

www.elsevier.com/locate/aej
www.sciencedirect.com

Developing an efficient deep neural network for automatic detection of COVID-19 using chest X-ray images

Sobhan Sheykhivand [a], Zohreh Mousavi [b], Sina Mojtahedi [c], Tohid Yousefi Rezaii [a,*], Ali Farzamnia [d,*], Saeed Meshgini [a], Ismail Saad [d]

[a] Biomedical Engineering Department, Faculty of Electrical and Computer Engineering, University of Tabriz, Tabriz, Iran
[b] Department of Mechanical Engineering, Faculty of Mechanical Engineering, University of Tabriz, Tabriz, Iran
[c] Department of Biomedical Engineering, Faculty of Engineering, Işık University, Istanbul, Turkey
[d] Faculty of Engineering, Universiti Malaysia Sabah, Kota Kinabalu, Sabah, Malaysia

Received 27 September 2020; revised 12 January 2021; accepted 14 January 2021
Available online 21 January 2021

KEYWORDS

COVID-19;
Pneumonia;
GANs;
X-ray Images;
CNN;
LSTM;
Transfer learning

Abstract The novel coronavirus (COVID-19) could be described as the greatest human challenge of the 21st century. The development and transmission of the disease have increased mortality in all countries. Therefore, a rapid diagnosis of COVID-19 is necessary to treat and control the disease. In this paper, a new method for the automatic identification of pneumonia (including COVID-19) is presented using a proposed deep neural network. In the proposed method, the chest X-ray images are used to separate 2–4 classes in 7 different and functional scenarios according to healthy, viral, bacterial, and COVID-19 classes. In the proposed architecture, Generative Adversarial Networks (GANs) are used together with a fusion of the deep transfer learning and LSTM networks, without involving feature extraction/selection for classification of pneumonia. We have achieved more than 90% accuracy for all scenarios except one and also achieved 99% accuracy for separating COVID-19 from healthy group. We also compared our deep proposed network with other deep transfer learning networks (including Inception-ResNet V2, Inception V4, VGG16 and MobileNet) that have been recently widely used in pneumonia detection studies. The results based on the proposed network were very promising in terms of accuracy, precision, sensitivity, and specificity compared to the other deep transfer learning approaches. Depending on the high performance of the proposed method, it can be used during the treatment of patients.

* Corresponding authors.
E-mail addresses: s.sheykhivand@tabrizu.ac.ir (S. Sheykhivand), zohreh.mousavi@tabrizu.ac.ir (Z. Mousavi), sna.mojtahedi@gmail.com (S. Mojtahedi), yousefi@tabrizu.ac.ir (T. Yousefi Rezaii), ali-farzamnia@ieee.org (A. Farzamnia), smeshgini@gmail.com (S. Meshgini), ismail_s@ums.edu.my (I. Saad).

Peer review under responsibility of Faculty of Engineering, Alexandria University.

https://doi.org/10.1016/j.aej.2021.01.011
1110-0168

1. Introduction

The novel coronavirus (COVID-19) became an epidemic in Wuhan, China, in December 2019 [1]. Today, the virus has become a serious public health problem worldwide [2]. The virus is also known as the SARS-COV-2 virus [3]. According to global health statistics, more than three million people worldwide are infected with the COVID-19 (until May 2020). In addition, more than 135,000 people have so far died from the virus [2,3]. Due to high virus infection, it is essential to control the disease, including rapid diagnosis and timely quarantine. Coronaviruses are a broad family of four types of viruses, including alpha-coronavirus, beta-coronavirus, coronavirus delta and gamma-coronavirus [4]. Up to now, seven out of 40 different species have been found capable of spread to humans in the Coronavirus family resulting in diseases such as common cold [5]. Past experiments have shown that both SARS and MERS viruses are passed on to humans from cats and camels. COVID-19 is believed to have been transmitted to humans from bats and anteaters [5].

The virus causes pneumonia to patients. Pneumonia infection in the lungs makes it difficult for the patient to breathe and causes the patient to die as the virus spreads. According to the latest guidelines published by the World Health Organization (WHO), reverse transcription-polymerase chain reaction (RT-PCR) or gene sequence for respiratory or blood samples must validate the diagnosis of coronavirus as the main indicator for hospitalization [6]. But it takes a long time for the relevant kits to detect a virus, in addition to the high time required for diagnosis, they are also less sensitive to the detection of the virus [7]. In addition, previous studies have shown that most doctors and nurses have been infected with the COVID-19 during salvia sampling based on RT-PCR kits [8]. These kits are also limited in the world and require transport costs. According to the content, the diagnosis based on these RT-PCR kits exposes doctors and nurses to the COVID-19 virus and is ultimately not cost-effective. Therefore, rapid diagnosis of COVID-19 is necessary to treat and control the disease [9].

The chest scan is another method used during the treatment of this diseases [10]. Computerized tomography (CT) and Digital Radiography (or standard 2D X-ray) scans are among the methods of chest imaging. DR is used to scan the body for the diagnosis of fractures, lung infections, pneumonia and tumors. CT is an advanced DR that provides clearer images of organs, bones, and tissue. However, CT scans are not available in all medical centers and are not as affordable as DR. For this reason, today physicians usually use DR in the first step of diagnosis. Using X-ray is a faster, easier, more affordable and more harmful method than CT [10]. After taking chest X-ray images, the doctor should visually diagnose bacterial, viral, COVID-19 and etc. infections. Due to exhaustion and the need for expert personnel, visual examination-based diagnosis is unpleasant, time-consuming and incorrect often results in low diagnosis accuracy. Also, the image consistency of chest X-ray has certain flaws, such as low contrast, overlapping organs and blurred boundary, which has a significant impact on the identification of chest X-ray pneumonia [11]. Based on the above-mentioned facts, automatic detection of the virus type (including COVID-19) based on chest images has gained a lot of attention in recent researches. Automatic detection of COVID-19 not only causes a fast diagnosis but also reduces the workload of doctors and is useful for timely treatment and patient mortality reduction.

Recently, various computational methods based on deep learning have been developed for the observation and analysis of the automatic detection of COVID-19 used X-Ray images, which will be discussed below.

Deep Learning is a fusion of methods for machine learning, primarily aimed at automatically extracting and classifying images while its applications are mostly encountered in the areas of medical image recognition, segmentation, and classification. The creation of deep learning applications in the last five years enables researchers to conduct a simple and profound analysis of the X-Ray scans [12].

Fie et al. [13] provided an automated algorithm based on deep learning approach for detecting infectious points in the lungs. Xiawi et al. [14] provided an initial screening model to distinguish between COVID-19 and viral pneumonia using CT imaging based on deep learning methods. Narin et al. [15] used X-ray images to automatically detect pneumonia based on three deep transfer learning networks (Inception V3, ResNet 50, Inception-ResNet V2). The ResNet 50 model has performed best among the other networks offered. The reported accuracy for the 2-stage classification of their proposed algorithm is 98%. Loannis et al. [16] used 1427 X-ray images to automatically classify three types of pneumonia (viral, bacterial and COVID-19). They used five deep transfer learning networks (VGG, MobileNet V2, Inception, Xception, ResNet V2) to classify three types of pneumonia. Their research shows that the VGG network has performed better than the other networks. The accuracy for 2-class (healthy and COVID-19) and 3-class (viral, bacterial and COVID-19) classification was also reported as 98.75 and 93.48, respectively. Loannis et al. [17] used deep convolutional neural networks to automatically classify pulmonary infections from X-ray images. The classification accuracy for 2-class and 7-class of pulmonary infections based on MobileNet is 99.18% and 87.66%, respectively. Pabira et al. [18] used a deep neural network approach to the automatic detection of MERS, SARS, and COVID-19 diseases from chest X-ray images. They used the ResNet 50 with Support Vector Machine (SVM) in their proposed model and achieved 95% accuracy in the classification of diseases. Khalifa et al. [19] used Generative Adversarial Networks (GANs) with fine-tuned deep transfer learning infections for automated detection of pneumonia from chest X-ray imagery. In their research, AlexNet, GoogLeNet, SqueezNet, and ResNet18 were selected as deep transfer learning models for the automatic detection of pneumonia. The accuracy reported by these researchers for classifying 2-class of pneumonia is approximately 99%. Huaiguang et al. [11] used deep neural networks in the fusion with random forest to automatically classify 2-class of pneumonia. They also used an adaptive median filter to remove the noise from the X-ray images. The final accuracy reported by these researchers for the classification of 2-class of pneumonia is 97%. Chuchan et al. [20] used X-ray images to automatically detect of pneumonia. In their proposed model, the researchers used five deep transfer learning networks (AlexNet, DenseNet, Inception V3, ResNet 18, and GoogLeNet) and data augmentation techniques. The final accuracy reported by these researchers for the classification of 2-class of pneumonia is 96%. Stephen et al. [21] proposed an efficient deep learning model for

Table 1 The number of images used for each group (healthy, covid-19, bacterial and viral).

Groups	Healthy	COVID-19	Bacterial	Viral
Number of Images	2923	371	2778	2840

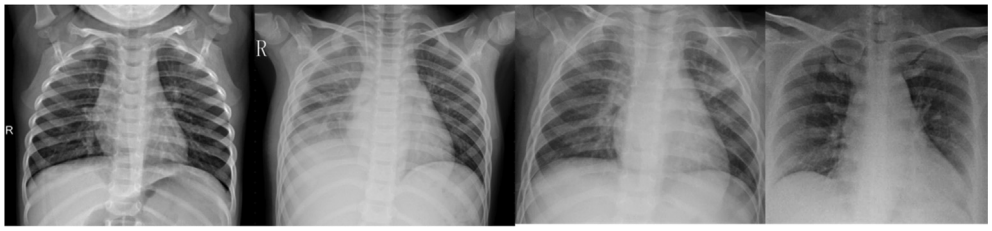

Fig. 1 The Chest X-ray images for four healthy, bacterial, viral, and COVI-19 groups (from left to right) respectively.

classifying pneumonia from chest X-ray images. Their network architecture consisted of 4-convolutional layers and 2-dense layers. The researchers found 93.7% accuracy in classifying two classes, healthy and pneumonia. Liang et al. [22] introduced a transfer learning method with a deep residual network to automatically classify two classes of pneumonia. Their proposed deep network consisted of 49-convolutional layers and 2-dense layers. Eventually, the researchers achieved 96.70% accuracy and 92.7% f-1 score. Noor et al. [23] Used deep learning networks to automatically detect 3 classes of pneumonia (viral, COVID-19, and, normal) based on chest X-ray images. Their proposed model for the feature extraction section consisted of 5 convolutional layers. The researchers also used the SVM, the K-nearest neighbors (KNN), and the decision tree for the classification section of their proposed network. The best performance of their proposed network based on SVM classifier was 98.97%, 89.39%, and 99.75%, and 96.72 accuracy, sensitivity, and specificity respectively. Brunese et al. [24] used X-ray images to automatically detect the COVID-19. They used an improved VGG16-transfer learning network to diagnose the two healthy and COVID-19 classes. The final accuracy reported by these researchers is about 98%. Also, the detection time based on their proposed modified network is about 2.49 s. Loannis et al. [25] introduced a new deep neural network to automatically detect COVID-19 based on chest X-ray images. They used a database of 1427 chest X-ray images to evaluate their algorithm. The best accuracy, sensitivity, and specificity achieved by these researchers for the classification of three different groups of healthy, COVID-19, and Pneumonia, were 96.78%, 98.66%, and 96.46% respectively. Wang et al. [26] used COVIDnet (based on CNN) to automatically detect COVID-19 using X-ray images. The researchers used the CXR database, containing 13,975 X-ray images of the chest, to evaluate their algorithm. The final accuracy achieved by these researchers was 93.3%. Foysal et al. [27] used three different models of CNN networks to automatically detect COVID-19 using X-Ray images. A database of 5863 X-ray images was used to evaluate their algorithm. The best performance (accuracy and precision) of the proposed method by these researchers was 97.56% and 95.34% respectively. Ardakani et al. [28] used deep transfer learning networks based on CT images to diagnose between two classes of COVID-19 and non-COVID-19. They used 10 deep transfer learning networks, including ResNet-50, VGG-16, SqueezeNet, ResNet-101, MobileNet-V2, AlexNet, VGG-19, Xception, ResNet-18, and GoogLeNet, and achieved promising results based on the Xception network. The final accuracy reported by these researchers based on the Xception network is about 99%. Jaiswal et al. [29] used chest CT images to automatically diagnose between the two classes (COVID-19 and non-COVID-19). In their research, they used a combination of a deep DenseNet transfer learning with convolutional networks. The final accuracy reported by these researchers for separating the two classes is reported to be about 96%. Horri et al. [30] used 3 types of medical imaging (X-ray, Ultrasound, and CT) to automatically detect the two classes of COVID-19 and healthy. In their research, they used an optimized deep VGG transfer learning network. The precision of their classification for three different imaging modes (X-ray, CT, and Ultrasound) was reported to be 86%, 84%, and 100% respectively.

Table 2 Scenarios considered in this work.

Case	Account
I	Healthy vs COVID-19
II	Healthy vs Pneumonia (Viral, Bacterial and COVID19)
III	Healthy vs COVID-19 vs Viral and Bacterial
IV	Healthy vs COVID-19 vs Bacterial
V	Healthy vs Covid-19 vs Viral
VI	COVID-19 vs Bacterial vs Viral
VII	Healthy vs COVID-19 vs Bacterial vs Viral

As is evident, most of the previous studies have used deep transfer learning approaches to classify between the two classes of pneumonia and healthy, and have achieved promising results. However, as can be seen, most of the previous research focused only on classifying the two healthy and pneumonia classes from the chest X-ray images (The number of studies conducted in a binary study for the automatic detection of COVID-19 is much higher than those based on multi-class studies). Obviously, in order to enter into recent research in the field of medical application, it is necessary to examine more

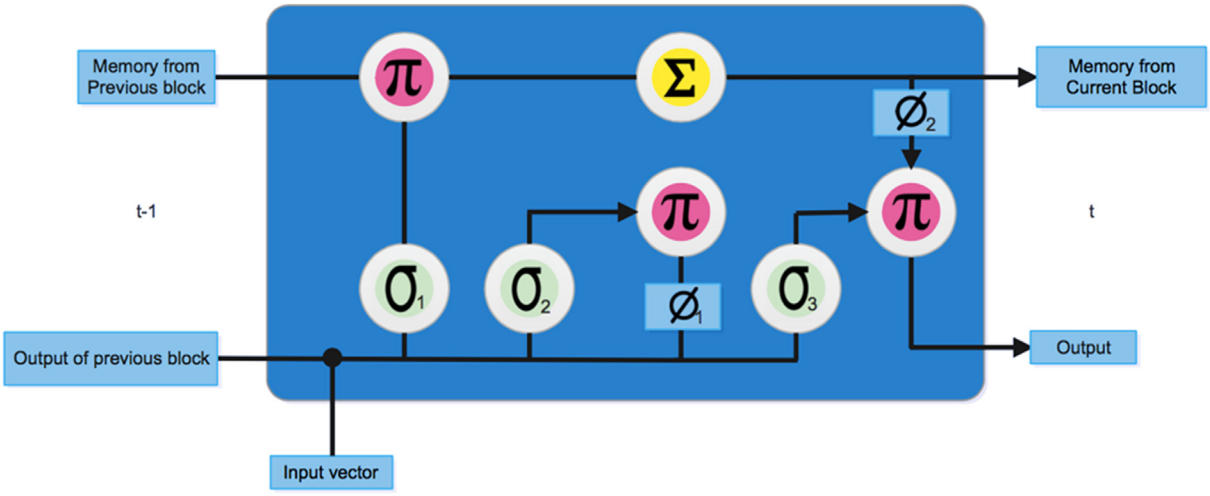

Fig. 2 The basic architecture of LSTM network.

comprehensive scenarios for the classification of different pneumonia states. In this study, 7 different scenarios of viral, bacterial, and COVID-19 from the chest X-ray images will be examined, provided that high accuracy is achieved in order to separate classes from each other.

In contrast to other methods that rely solely on transfer learning approaches or traditional handcrafted techniques to achieve remarkable classification performance, In the proposed method GAN networks are used together with a fusion of the deep transfer learning and LSTM networks (proposed DNN model) to train and separate 2 to 4 classes in 7 different and functional scenarios according to healthy, viral, bacterial, and COVID-19 groups. In the proposed DNN, at first preprocessing operations are performed on the chest X-ray images based on GANs; then a fusion of a deep transfer learning (base part) and LSTM (head part) network is used to train and classify different groups of pneumonia. The proposed DNN can be viewed as an end-to-end classifier in which there is no need for a process of selection/extraction of features and the necessary features of each class would be learned automatically with a proposed DNN.

The remainder of the paper is divided as follows: Section 2 outlines the specifics of the related database based on the chest X-ray image and the underlying mathematical context of the GAN, CNN, and LSTM networks. In Section 3, the suggested method is presented. The results of the simulation and comparison of the proposed method with the other conventional methods are set out in Sections 4 and 5; the conclusion is finally set out in Section 6.

2. Materials and methods

In this section, the database used is first described based on the chest X-ray images, then the mathematical background related to the deep networks including CNN, LSTM, and GANs will be provided.

2.1. Chest X-ray databases

For the experiment, six different reputable and reliable databases based on chest X-ray images were used. Recently, these databases have been widely used in studies involving automatic detection of COVID-19 [31–36]. These datasets consist of the posterior-anterior chest image of patients with pneumonia. These chest X-ray images include four different categories of healthy, viral pneumonia, bacterial pneumonia, and COVID-19 pneumonia. The number of each X-ray images in each group is shown in Table 1. Fig. 1 shows four different categories of the chest X-ray images. As can be seen from Fig. 1, there is no noticeable difference between viral groups and COVID-19, and this is not visually recognizable.

In this study, we have considered seven different scenarios for the chest X-ray images to separate 2 to 4 classes according to healthy, viral, bacterial, and COVID-19 groups. The scenarios considered in the study are shown in Table 2. These scenarios are very useful in the field of medicine.

2.2. Convolutional neural network (cnn)

CNNs are one of the most important deep learning methods in which several layers are trained in a powerful way. These networks are highly efficient and are now recognized as one of the most common methods for various applications of machine vision and medical image processing. In general, a convolutional neural network consists of three main layers: the convolution layer, the pooling layer, and the fully connected (FC) layer which different layers perform different tasks. Details of each layer are provided below [37,38]:

- Convolution layer: using some imaging techniques such as sharpening, smoothing, noise cancellation and edge detection, the image is used as input and extracts its specific specifications.
- Pooling layer: reduces the dimension of the feature matrix and retains important features.
- Fully connected layer: injects the result of the flattening layer into one or more neural layers to make a classification prediction [39–42].

2.3. Long short-term memory (lstm)

Recurrent neural networks (RNNs) are powerful deep learning networks that are commonly used for sequential data. These

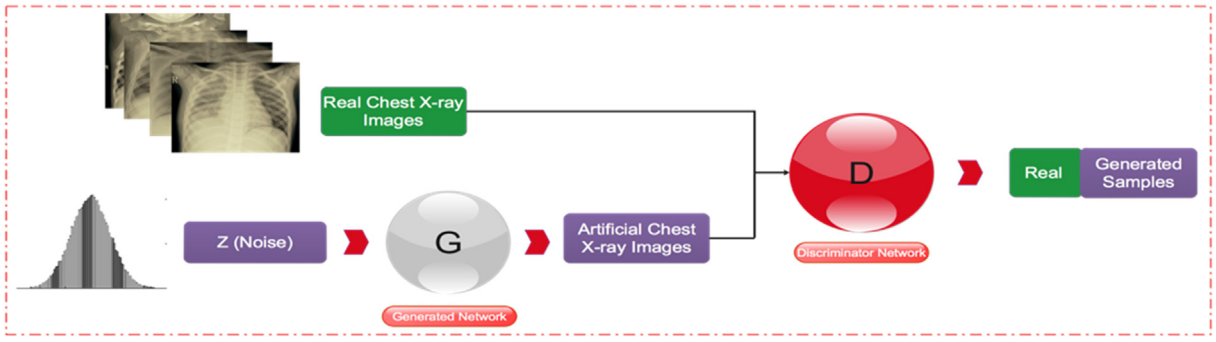

Fig. 3 Graphical representation of the GAN networks.

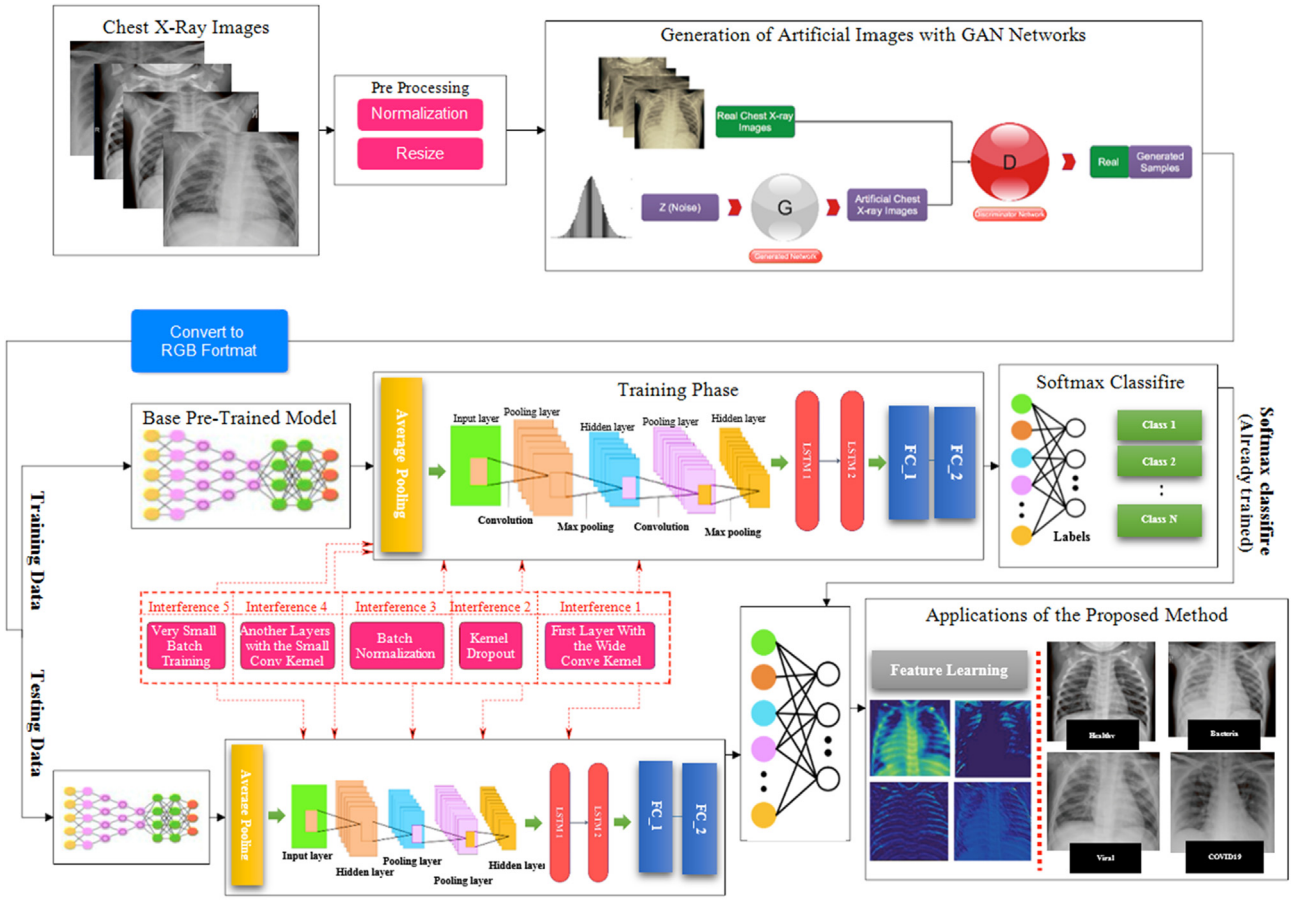

Fig. 4 The block diagram related to the proposed DNN model.

networks were first used for the processing and recognition of natural languages. In fact, language data can be thought of as sequences such as words (sequence of particles), phrases (sequence of words), and documents (sequence of sentences). RNNs have two main advantages that have been used in the proposed architecture: first, these networks have benefits in the analysis of nonlinear time series compared to other linear methods. Second, with the efficient architecture of RNNs, the data input dimension can be reduced, ultimately reducing the computational load of the algorithm and facilitating the process of using the algorithm for real-time systems. Some applications need only new information for training, while others may request more information from the past. In learning, the standard RNNs lag as the distance between the previous knowledge needed and the point of requirement increases to a large extent. But luckily, long short-term memory (LSTM) Networks, a special type of RNN are able to learn such scenarios. These networks were introduced by Hochreiter and Schmidhuber in 1997. The LSTM is good at remembering information for a long time. As previous information may further affect the accuracy of the model, the use of LSTM has become a widely used choice for researchers [43–46]. Fig. 2 shows the basic architecture of LSTM network.

Module LSTM has four layers of neural networks that interact with each other in a unique way. As shown in Fig. 2, the LSTM module has three gate activation functions

and two output activation functions. The symbols (π) and (Σ) represent the multiplication and addition of elements, respectively. The concatenation operation is also indicated in the symbol (•) bullet. The basic component of the LSTM module is its cell state; the memory line running from the previous block (S_{t-1}) to the current block (S_t). This allows information to flow down the line directly. The network can also determine the amount of the previous information flow that is controlled through the first layer (σ_1). The operation performed in this layer is described in Equation (1). The new information stored in the cell state is calculated using two layers of the network. A sigmoid layer (σ_2) that decides to update the values (I_t) in Equation (2) and tanh layer (φ_1) that develops the vector of the new candidate values (S_t) as shown in Equation (3). In this state, a combination of both is added. Finally, cell status is updated using Equation (4) [44–46].

$$cf_t = \sigma_1(W_{cf}.[O_{t-1}, x_t + b_{cf}]) \tag{1}$$

$$I_t = \sigma_2(W_I.[O_{t-1,}x_t) + b_1]) \tag{2}$$

$$S_t = tanh(W_s.[O_{t-1}.x_t + b_s]) \tag{3}$$

$$S_t = cf_t \times S_{t_1} + I_t \times S_{t-1} \tag{4}$$

In this research, a combination of CNN and LSTM networks was used to automatically detect pneumonia (healthy, viral, bacterial and COVID-19) from chest X-ray images.

2.4. Generative adversarial networks (GANS)

GANs were first introduced by Lan Goodfellow in 2014 [47]. In recent years, these networks have received a great deal of attention in the field of deep learning. GANs using convolutional neural network architecture can learn the dataset (such as the chest X-Ray images) used in experiments and generate a new and real dataset that is not available in the previous dataset. Among the applications of this network in the field of machine vision, we can mention the production of video and video content, feature extraction in the form of unsupervised learning, image coding and super-resolution imaging, analysis, and synthesis of speech.

The GANs consist of two main generator (G) and discriminator (D) networks. These two components are acting exactly opposite each other. The generator starts its work by creating noisy images from input data. The generator has a duty to produce images as natural and as real as possible. The discriminator is responsible for distinguishing the images from the artificial images. For example, in the present study, the

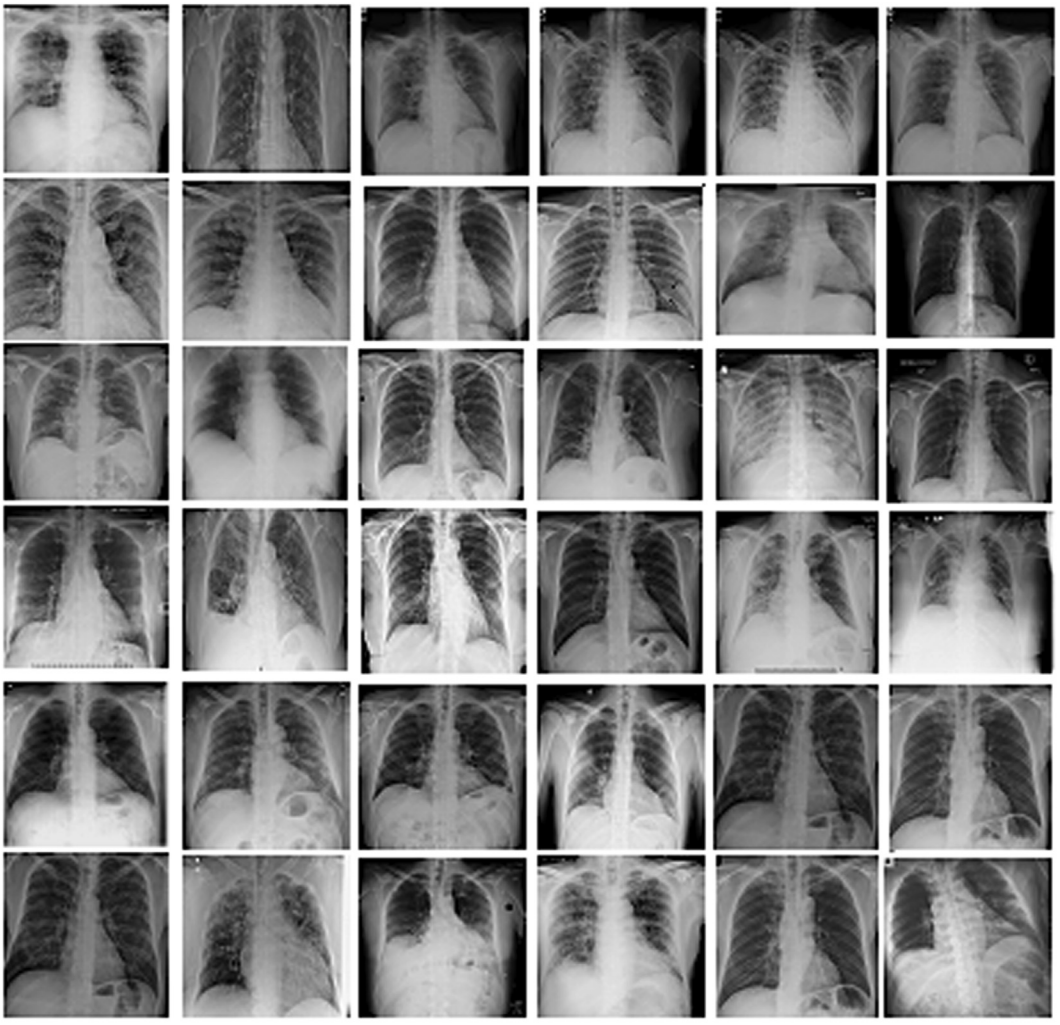

Fig. 5 Artificial images generated by the GAN networks in order to balance the samples of the COVID-19 group.

discriminator must look at the chest X-ray images produced by the generator in order to determine if these images look natural enough. In these networks, D indicates the probability that the input is part of the original data. Network D is taught in order to maximize the accuracy of distinguishing the original data from the generated data. On the other, the G network is simultaneously trained to mislead the D network, which minimizes the following function:

$$\log(1 - D(G_{(Z)})) \tag{5}$$

Finally, the following function is minimized:

$$\min_{G} \max_{D} V(G, D) = E_{x-Pdata}[logD(x)] + E_{Z_{PZ_{(Z)}}}[\log(1 - D(G(z))] \tag{6}$$

According to the above Equation, D is extracted in such a way that it can correctly distinguish between real and artificial data. This Equation cannot be resolved as a closed-form and must be resolved by means of repetitive and numerical methods [47]. Fig. 3 shows the described contents graphically.

In this paper, samples from each group of the X-ray images are balanced using GAN networks at first; Then, we used a fusion of deep transfer learning (base part) and LSTM (head part) networks to automatically classify the pneumonia (healthy, viral, bacterial and COVID-19) from chest X-ray Images. We'll see that these two networks' fusion will increase the accuracy and decrease the oscillation. In Section 3, details of each move will be clarified.

3. Suggested DNN model

In this section, the specifics of the suggested model will be presented based on deep networks for the automatic classification of pneumonia. This section is organized into three subsections, including pre-processing, proposed network architecture and data allocation. Fig. 4 displays the block diagram of the suggested DNN model. According to the proposed block diagram, the chest X-ray images first enter the pre-processing stage. Operations such as normalization and resizing are performed on images in this part. In the second step, the data will be entered into the GAN network in order to balance the data of each class. The data is then entered into the proposed DNN for automatic feature selection/extraction and classification. Finally, according to the proposed DNN, the chest X-ray images will be classified into four classes: healthy, COVID-19, viral and bacterial. In the following, more detail will be provided on each step of the proposed method.

3.1. Pre-processing

In this section, the pre-processing operations on chest X-ray images are described in four different steps. Due to the fact that original X-ray images received from six different databases had different colors and formats, first all images have been normalized between zero and 1. Second, the images have been resized to a size of 224 × 224 pixels. The resize is done to facilitate experimentation as it allows for a considerable decrease in computational time. As shown in Table 1, the number of chest X-ray images of each group is not equal due to the limitation of the COVID-19 samples. This imbalance of classes will lead to over-fitting problems and poor classification performance. The GAN networks were used to overcome this problem in the third step. Due to the small number of COVID-19 samples in Table 1, GAN networks were used to artificially increase the number of samples in the COVID-19 group. This process helps to solve the problems of overfitting and enhances the ability to generalize the model during training. The generator network takes a vector of 100 random

Table 3 The Number of X-ray images before and after using GAN networks.

Groups	Healthy	COVID-19	Bacterial	Viral
Before GANs are Used	2923	371	2778	2840
After GANs are Used	–	2471	–	–
Total	2923	2842	2778	2840

Table 4 Details of the modified part of training phase of the proposed deep neural network architecture.

L	Layer type	Activation function	Output Shape	Size of Kernel and Pooling	Strides	Number of filters	padding
0–1	Average Pooling 2-D	–	(None, 2048, 1, 1)	4 × 4	1 × 1	–	**no**
1–2	Convolution1-D	Leaky ReLU	(None, 256, 16)	120 × 1	8 × 1	16	**yes**
2–3	Max-Pooling1-D	–	(None, 128, 16)	2 × 1	2 × 1	–	**no**
3–4	Convolution1-D	Leaky ReLU	(None, 128, 32)	3 × 1	1 × 1	32	**yes**
4–5	Max-Pooling1-D	–	(None, 64, 32)	2 × 1	2 × 1	–	**no**
5–6	Convolution1-D	Leaky ReLU	(None, 64, 32)	3 × 1	1 × 1	32	**yes**
6–7	Max-Pooling1-D	–	(None, 32, 32)	2 × 1	2 × 1	–	**no**
7–8	Convolution1-D	Leaky ReLU	(None, 32, 64)	3 × 1	1 × 1	64	**yes**
8–9	Max-Pooling1-D	–	(None, 16, 64)	2 × 1	2 × 1	–	**no**
9–10	LSTM	Leaky ReLU	(None, 100)	–	–	–	
10–11	LSTM	Leaky ReLU	(None, 100)	–	–	–	
11–12	Fully-connected	Leaky ReLU	(None, 80)	–	–	–	
12–13	Fully-connected	Softmax	(None, 2–3-4)	–	–	–	

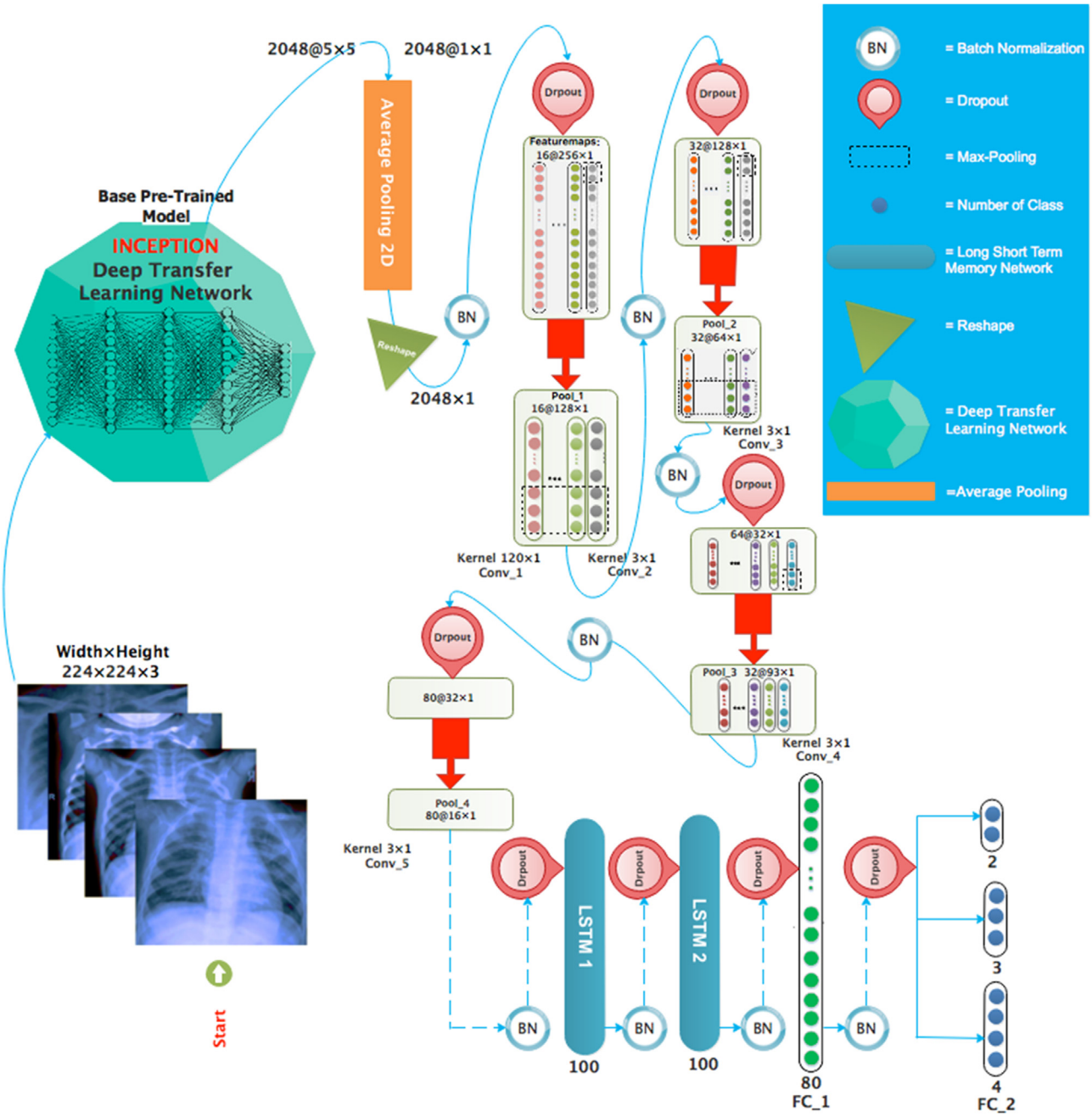

Fig. 6 Graphical representation of the proposed network architecture including the base part (base pre-trained model) and modify part.

Table 5 Number of parameters and samples in the proposed DNN model for each scenario.

Scenarios	No. of Samples	No. of Parameters
I	5765	23,070,030
II	5845	23,070,030
III	8687	23,070,131
IV	8543	23,070,131
V	8605	23,070,131
VI	8460	23,070,131
VII	11,383	23,070,232

Table 6 The X-ray images data allocation in the proposed DNN model for training, validation, and test sets.

Scenarios	No. of Samples for Training (70%)	No. of Samples for Validation (10%)	No. of Samples for Testing (20%)
I	4035	576	1153
II	4092	584	1169
III	6081	868	1738
IV	5980	854	1709
V	6024	860	1721
VI	5922	846	1692
VII	7968	1138	2277

Fig. 7 The results of the confusion matrix for each of the scenarios.

entities from a uniform distribution as input and outputs a signal of size 50,176 (224 × 224). The network architecture consists of four dense fully-connected layers (256, 512, 1024, and 50,176) where each layer is followed by a batch-normalization layer. We used Leaky-Relu as the activation function in hidden layers and tanh activation function at the end of the network. The discriminator network takes the input of size 50,176 and outputs a decision (if the images are real or fake). In this network, four dense fully-connected layers are used (1024, 512, 256, and 1), where each layer is followed by a dropout layer. We used Leaky-Relu as the activation function in hidden layers and the sigmoid activation function at the end of the network. The training process is performed by Mean Squared Error (MSE) [48] cost function and binary cross entropy optimizer [49] with a learning rate of 0.0002 and batch size 10 for 1000 epochs in GAN network. Fig. 5 shows the artificial images generated by the GAN networks for the COVID-19 group. Table 3 shows the number of chest X-ray images before and after using the GAN networks. According to Table 3, after using GAN networks, the number of samples in the COVID-19 group is almost equal to that of other groups. In the fourth step, all images are converted to

an RGB format; so, all images have been resized to a size of $224 \times 224 \times 3$.

3.2. Proposed architecture

In the suggested architecture, a model was designed based on the pre-trained Inception V4 network to improve the overall the Inception V4 [50] network structure for feature extraction. We improved the Inception V4 network and fine-tuned with pre-trained weights the new Inception network. During the training process, the original Inception part (base part) was not trained, and only the improved part (head part) was trained.

In the proposed network, the pre-trained Inception V4 network fusion with a modified part contains 3 convolution 1D, 2 LSTM, and 2 fully connected layers. For the implementation of the suggested DNN, a cross-library in Python programming language is used. The architecture of the improved component has also been selected as follows: I. An Average Pooling layer that followed by batch normalization and dropout layers. II. A convolutional layer with a nonlinear Leaky-Relu function, followed by batch normalization and dropout layers with a

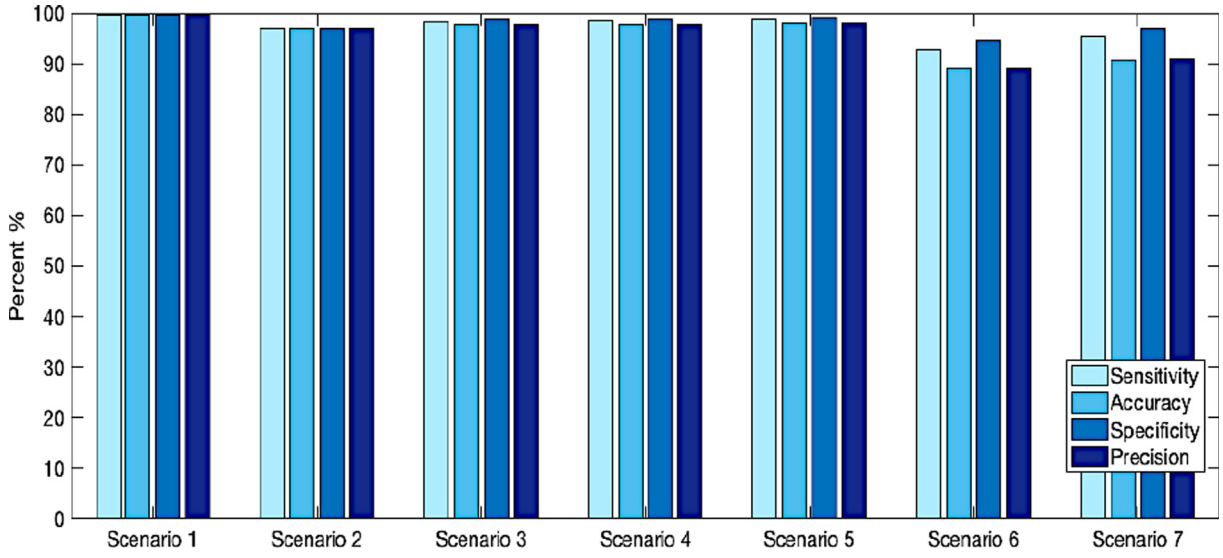

Fig. 8 The bar-chart diagram for the classification of the all scenarios (I-VII).

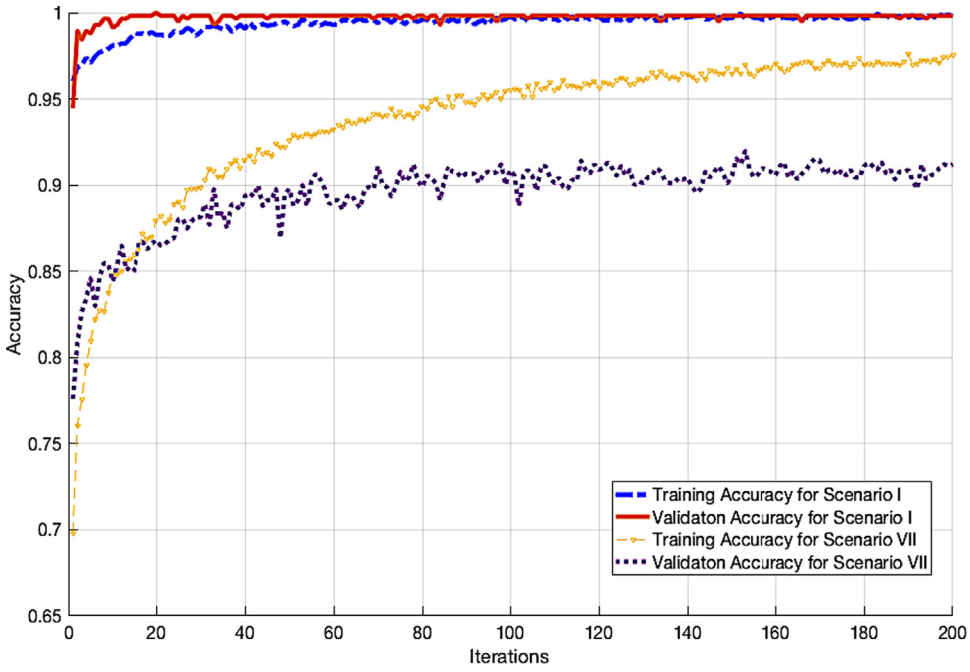

Fig. 9 The Accuracy of the proposed network for the classification of first and seventh scenarios for training and validation data in 200 iterations.

max-pooling layer. III. The Architecture of the previous phase is repeated 2 times. IV. The previous output of the architecture connects to the 2 LSTM layers with nonlinear Leaky-Relu functions that are accompanied by batch normalization and dropout layers. V. A 2D matrix is attached to the output of the previous architecture. VI. To access the output layer, two fully-connected layers are used. Table 4 displays the specifics about the suggested architecture of the DNN. As shown in Table 4, the reduction in the dimensionality of the hidden layers continued from $224 \times 224 \times 3$ to 80. Finally, the selected feature vector was linked with the nonlinear Softmax function to the fully connected layer. The proposed DNN model is influenced by two main interferences, the wide kernel in the first convolution layer and the small kernels in the remaining updated component layers. The first interference is more capable of removing high-frequency noises compared to small kernels, and the second interference is more capable of reflecting the input features; thus, enhancing the overall network efficiency. Fig. 6 shows the graphical architecture of the proposed deep neural network.

3.3. Training and evaluation

All hyper-parameters for the proposed DNN model are carefully modified to achieve the best convergence rate and to evaluate these hyper-parameters, the trial-and-error process is followed. Finally, the training process is carried out with a learning rate of 0.001 and batch size 10 through the Mean Squared Error (MSE) cost function and RMSProp optimizer. Table 5 shows the total number of parameters and samples for each of the scenarios. Also, Table 6 shows samples for training, validation, and test sets for each scenario. According to Table 6, 80 percent are randomly chosen for training and the remaining 20 percent are selected as the test set. In addition, 10 percent of the data are used for validation for the training collection.

4. Simulation results

In this section, the results of the suggested DNN model for automatic classification of pneumonia will be presented. Then, the results of the proposed method will be compared with recent methods. All experiments were performed on the Google Collaboratory system using 14 GB of RAM and the Tesla K80 GPU graphics card. Fig. 7 shows the confusion matrix of all scenarios. According to Fig. 7, the accuracy of all scenarios is more than 90%, except one of them. According to Fig. 7, the classification accuracy of the proposed algorithm for two groups (healthy vs COVID-19) is above 99%. As can be seen from the confusion matrix in Fig. 7, for the first scenario, which is related to the classification of two classes of COVID-19 and healthy, 564 samples of COVID-19 from the test set were correctly identified by the proposed network, while only 2 samples were misdiagnosed. Furthermore, Fig. 8 shows the bar-chart diagram of sensitivity, precision, specificity, and accuracy for classification of all scenarios. In addition to the accuracy obtained, the precision, sensitivity and specificity values for classification of all scenarios are very promising, as shown in Fig. 8. It is also observed that the results obtained in terms of accuracy, sensitivity, accuracy, and specificity for the separation of the healthy group from COVID-19 pneumonia (scenario I) are approximately 99%; This indicates the perfect performance of the proposed algorithm. Also, Fig. 9 shows the accuracy of the proposed networks for the classification of scenarios I and VII for training and validation data in 200 iterations. As can be seen from Fig. 9, the accuracy of the classification for the first and seventh scenarios reaches 99% and 91%, respectively. It

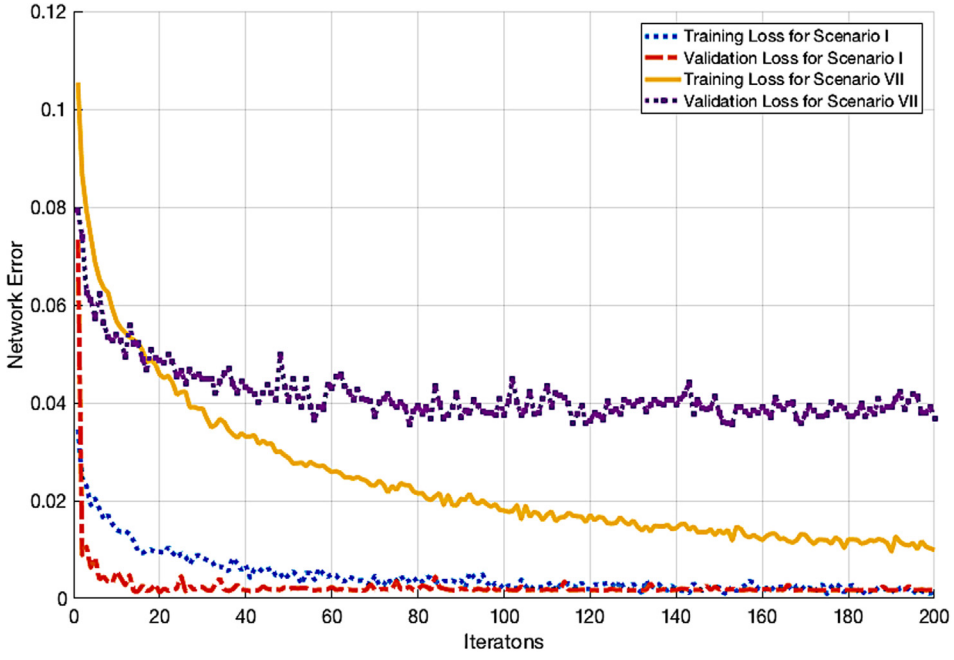

Fig. 10 The network error of the proposed network for the classification of first and seventh scenarios for training and validation data in 200 iterations.

is also observed the steady-state value for the classification accuracy of the first and seventh scenarios from about 80th and 100th iteration, respectively. Fig. 10 shows the loss function for the classification of the first and seventh scenarios. As we can see from Fig. 10. The network error for first scenario classification decreases as the number of iterations rises and approaches its steady-state value from about the 80th iteration. According to Fig. 10 the network error for scenario I will eventually be reduced from 0.098 to 0.0052. Also, it can be seen from Fig. 10 the steady-state value for classification of seventh scenario from about 95th iteration. According to Fig. 10 the network error for scenario VII will eventually be reduced from 0.08 to 0.03. To further analyze the proposed method, the t-SEN diagram for the classification of all scenarios for the last FC layer is shown in Fig. 11. As shown in Fig. 11, almost all of the COVID-19 samples were separated from the healthy ones in the first scenario.

This is evidence of the high performance of the proposed DNN architecture. The number of positive and negative validation set samples used for evaluating the efficiency of the model is unbalanced; Therefore, the Receiver Operating Characteristic (ROC) curve analysis of our model for the classification of all scenarios is shown in Fig. 12 in order to determine the high performance of the suggested method.

For further analysis, the performance of the proposed DNN model is compared to other deep transfer learning networks that have recently been used in pneumonia diagnostic studies. From deep transfer learning networks including MobileNet [51], VGG16 [52], Inception V4 [53] and Inception-ResNet V2 [54] have been used for comparison purposes for classification of seventh scenarios. The networks selected for comparison have been used as a proposed algorithm in recent studies for the identification of COVID-19. According to Fig. 13, the reliability of the proposed DNN, MobileNet, VGG16, InceptionV4, and Inception-ResNetV2 reaches 91%, 87.7%, 84.6%, 82.4, and 87.5%, respectively after 200 iterations. Fig. 14 also shows the network error of the proposed DNN as compared to the MobileNet, VGG16, Inception V4, and Inception-ResNet V2 networks. According to Fig. 13 and 14, it is observed that the proposed DNN has the highest accuracy and the lowest error compared to other networks for the classification of pneumonia. The confusion

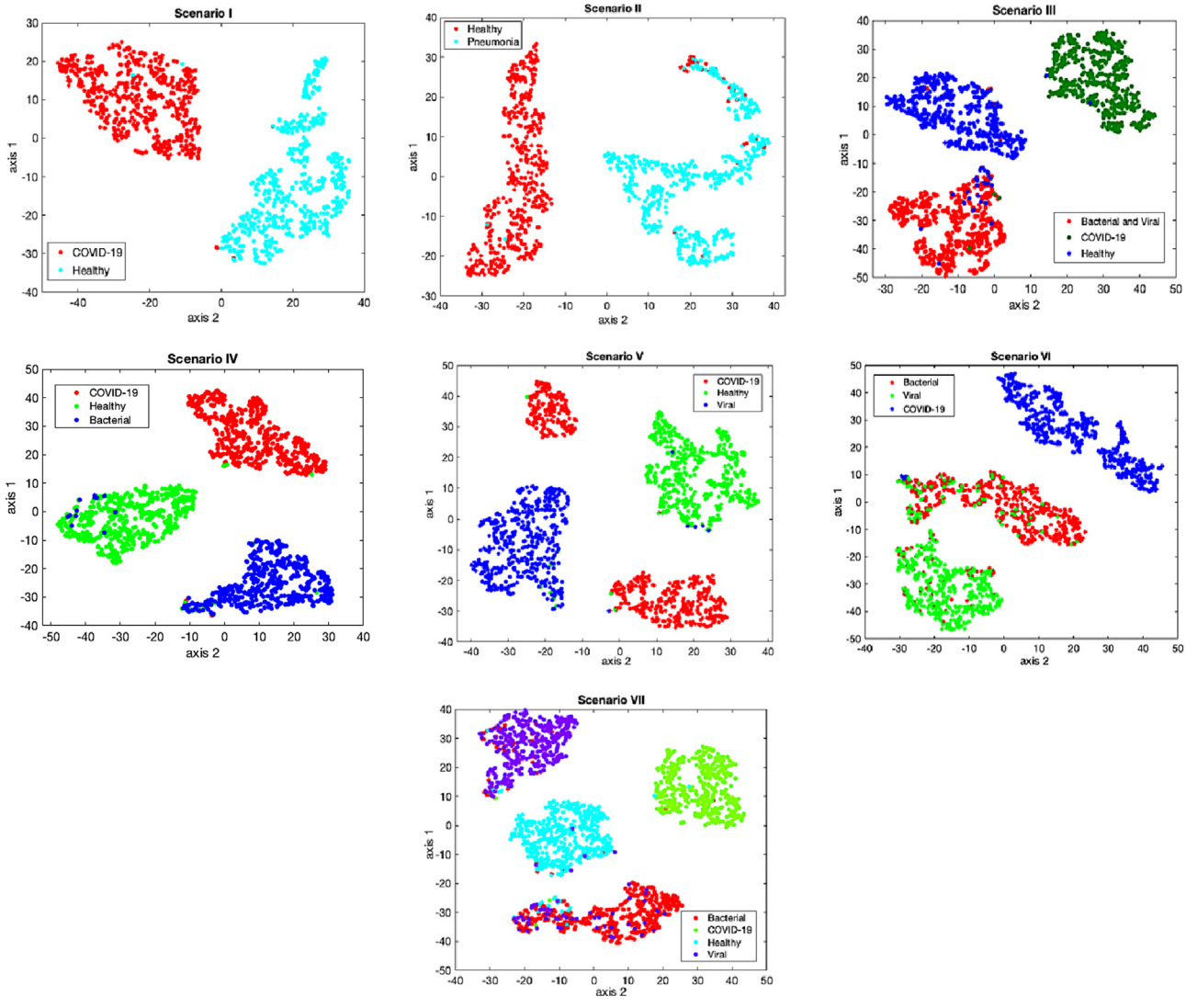

Fig. 11 The t-SEN chart for the all scenarios classification.

matrix, the ROC analysis and the t-SEN chart of the last layer of each of the compared networks for the seventh scenario classification are also shown in Fig. 15. According to Fig. 15, it can be seen that the compared networks have been able to differentiate between COVID-19 samples with lower accuracy than the proposed DNN model, but these networks have not been very successful in separating other pneumonia, including bacterial from viral samples. Also, Fig. 16 shows the bar-chart diagram of specificity, precision, sensitivity, and accuracy for each of the compared deep transfer learning networks. Therefore, according to the above facts, the proposed DNN model has been able to provide the best performance compared to the other networks for classification of the pneumonia (including COVID-19) from the chest X-ray images.

Table 7 shows the computational complexity of the running time for the training and testing process of the proposed DNN for each of the scenarios. The computational complexity for the classification of the seventh scenario for each of the comparative networks in 200 iterations is also shown in Table 8. According to Table 8, the proposed network does not have the lowest test running time compared to the other networks, but given the good performance of the proposed network in terms of accuracy, precision, sensitivity and specificity, the test running time for the proposed network is still promising.

White Gaussian noise was applied to raw chest X-ray images in different SNRs to test the proposed algorithm against observation noise. The noise added to the images in the various SNRs (−4 to 20 dB) is shown in Fig. 17. The accuracy of the classification of each network (proposed DNN

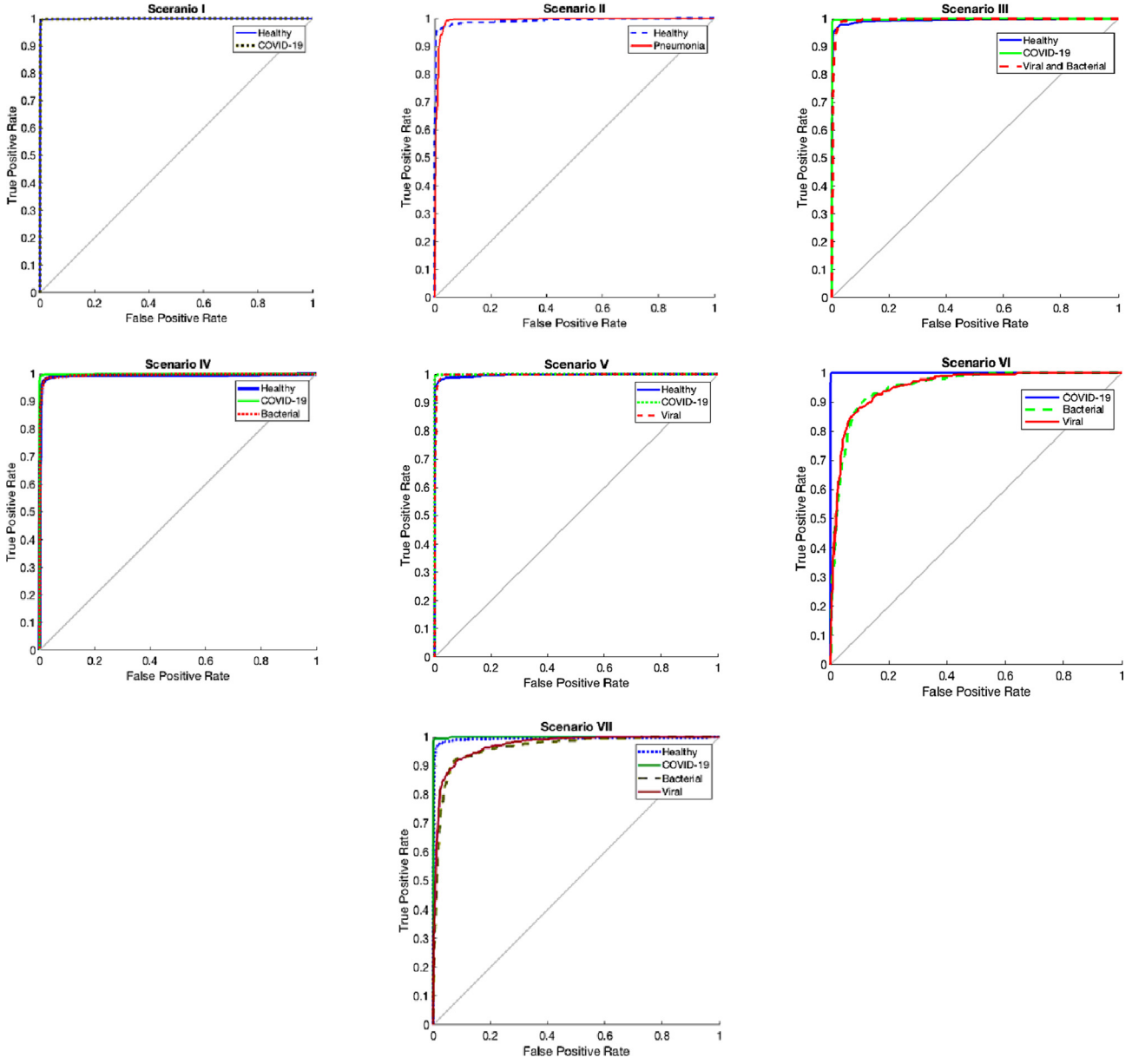

Fig. 12 The ROC analysis for the classification of each scenario.

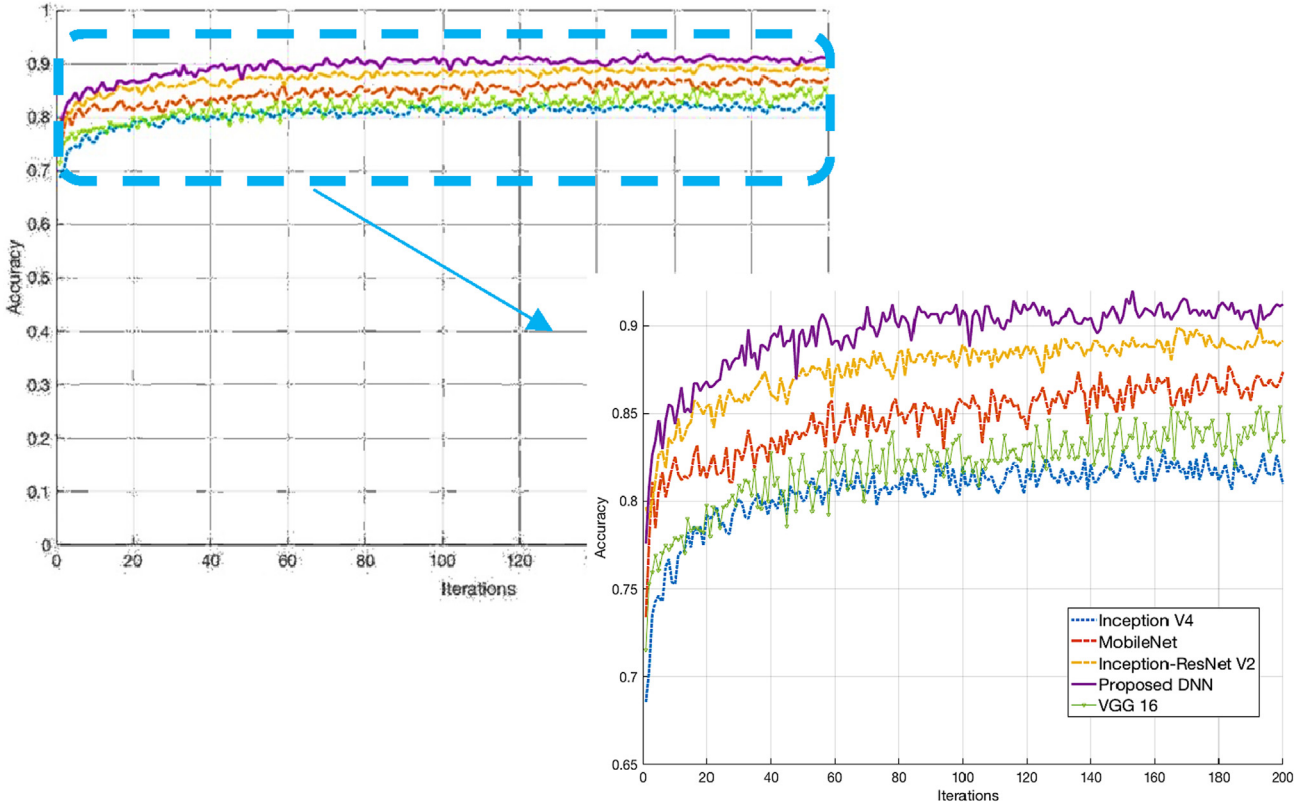

Fig. 13 The accuracy of the suggested network compared to the Inception V4, VGG16, Inception-ResNet V2 and MobileNet networks for classification of the seventh scenarios (Healthy, COVID-19, Bacterial and Viral).

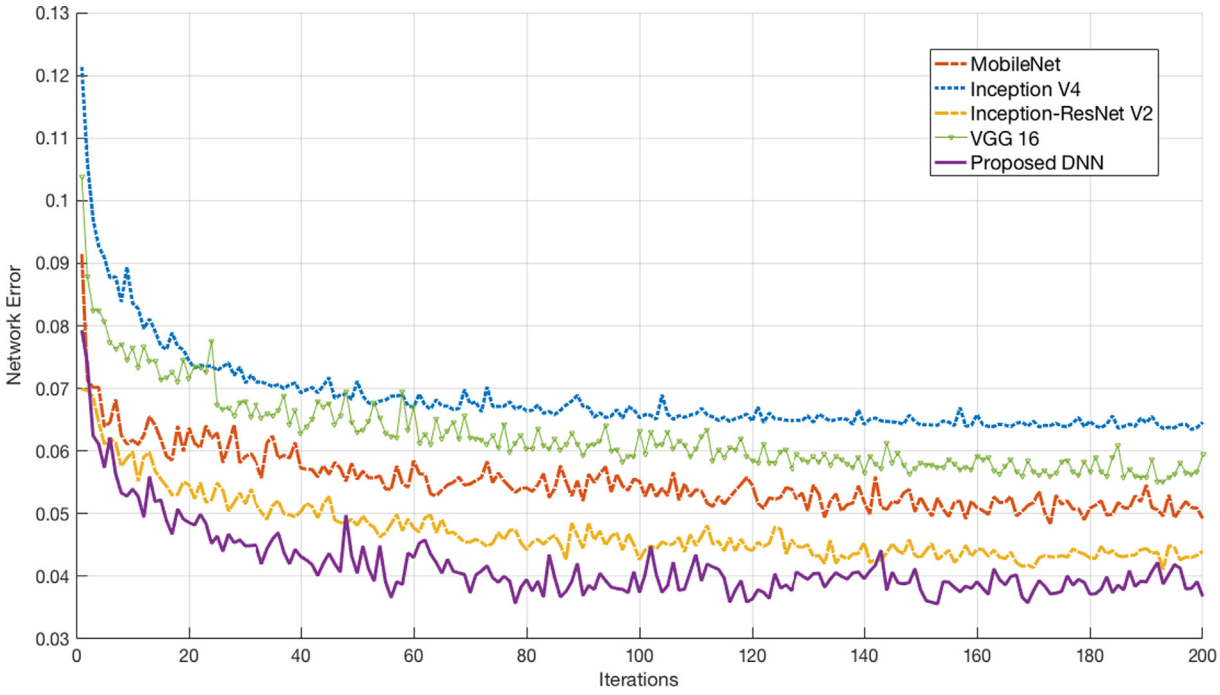

Fig. 14 The network error of the proposed network compared to the Inception V4, VGG16, Inception-ResNet V2 and MobileNet networks for classification of the seventh scenarios (Healthy, COVID-19, Bacterial and Viral).

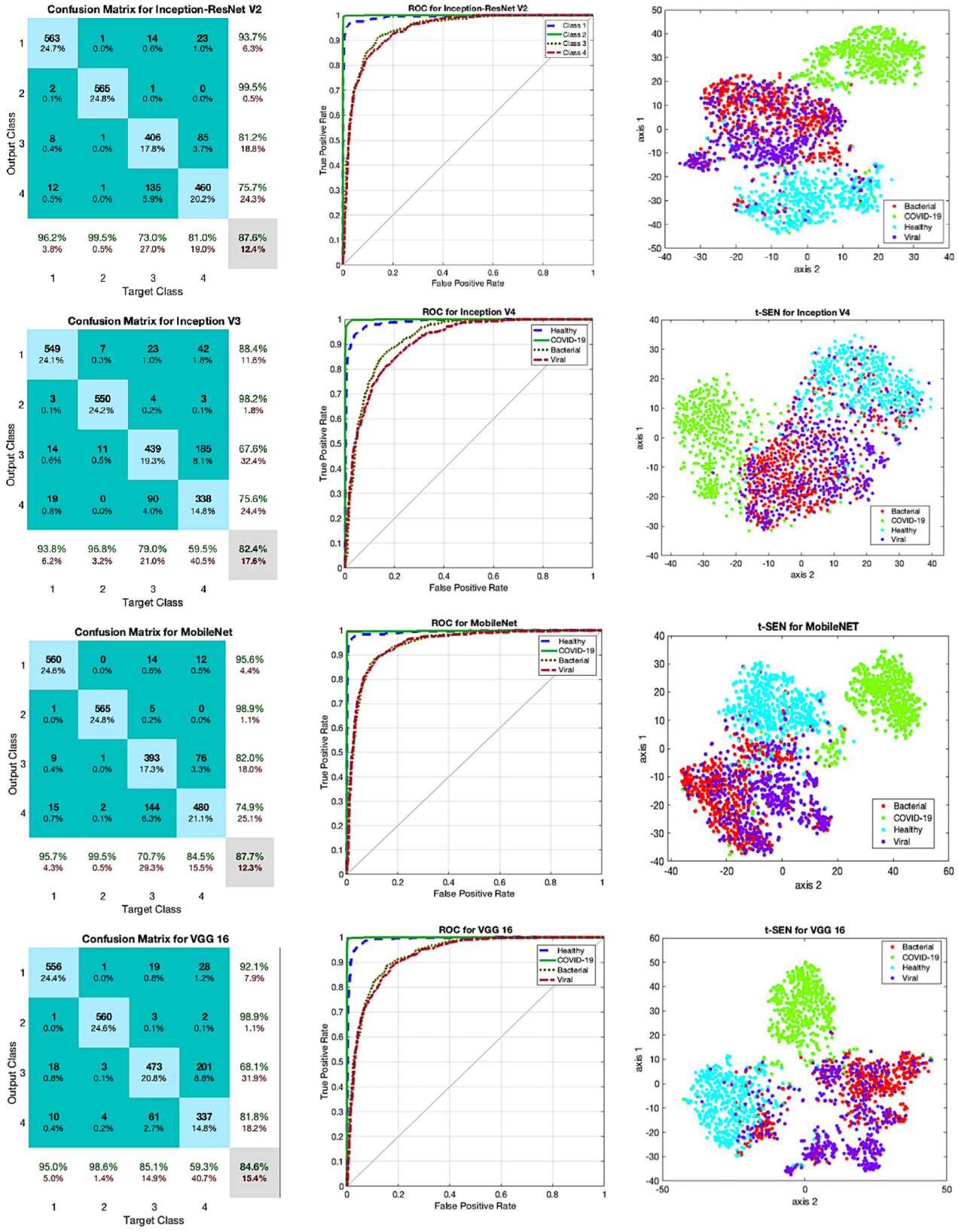

Fig. 15 The confusion matrix, ROC analysis and t-SEN chart for the classification of seventh scenarios for each of the networks compared.

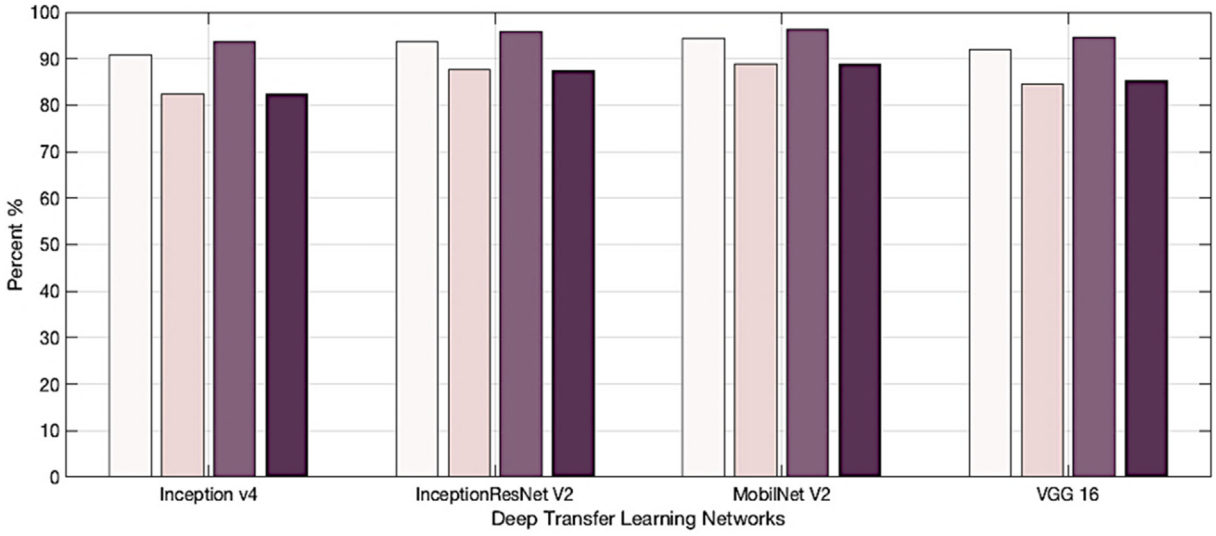

Fig. 16 The sensitivity, accuracy, precision and specificity for the classification of seventh scenarios for each of the compared networks.

Table 7 The X-ray images data allocation in the proposed DNN model for training, validation, and test sets.

Case	Train (for each iteration)	Test (for all of the data)
I	15 s	3 s
II	14 s	3 s
III	23 s	5 s
IV	21 s	5 s
V	23 s	5 s
VI	21 s	5 s
VII	29 s	7 s

model, MobileNet, VGG16, Inception V4 and Inception-ResNet V2) for each SNR is reported in Fig. 18. As can be seen, the classification accuracy of the proposed DNN is considerably robust to the measurement noise in a wide range of SNR, so that the accuracy is still more than 80% for SNR 0–20 dB; This is due to the fact that in the proposed network architecture, the wide kernel in the first convolution layer and small kernels in the remaining modify part have been used. Based on the available evidence, the proposed algorithm may also be used for low-contrast and noisy X-ray images.

Despite the good performance of the proposed method for the classification of pneumonia based on chest X-ray images, this work, like other studies, also has limitations. Due to the limitations of the COVID-19 samples, a clinical validation study based on a larger dataset with more COVID-19 samples is needed to check the performance of the proposed network. Furthermore, with a realistic review, in order to include the proposed method in the field of application, it is necessary to examine several scenarios, including SARS and MERS diseases, unfortunately, have not been carried out due to lack of access to these databases. However, with the extension of the suggested method, this method can be used in the near future as a medical assistant to diagnose a variety of diseases (including COVID-19) from chest X-ray images with an accuracy of more than 90%. As a result, the use of the proposed method will be reducing the use of expert human resources, reduce the error of visual recognition, reduces infection with the virus, and reduces mortality.

5. Discussion

The advantages and disadvantages of the proposed method are examined in this section. Table 9 compares the performance of the proposed method with recent research. As can be seen from Table 9, the suggested method is superior to recent methods in terms of the number of classes classified and the scenarios studied.

The distribution of data for training and evaluation sets is the same in all previous studies. However, due to variations in datasets, techniques, and different simulation environments, it is important to be aware that a one-to-one comparison is not feasible. According to available evidence, many people have been infected with COVID-19 so far, however, the number of X-ray samples of people infected with COVID-19 is small and there is no comprehensive database for chest X-ray images of COVID-19. Based on the review and description of the experimental data related to this study and other studies, it

Table 8 Comparison of the proposed network's computational complexity with MobileNet V2, Inception-ResNet V2, InceptionV4, and VGG16 for classification of the fourth scenario (Healthy, COVID-19, Bacterial and Viral) in 200 iterations.

	P-M		MobileNet V2		Inception-Resnet V2		Inception V4		VGG16	
Case	Train	Test	Train	Test	Train	Test	Train	Test	Train	Test
VIII	5800	7 s	2200	3 s	10,800	14 s	4800	6 s	6600	8 s
I	3000	3 s	1200	1.5 s	5200	7 s	2400	3 s	3000	4 s

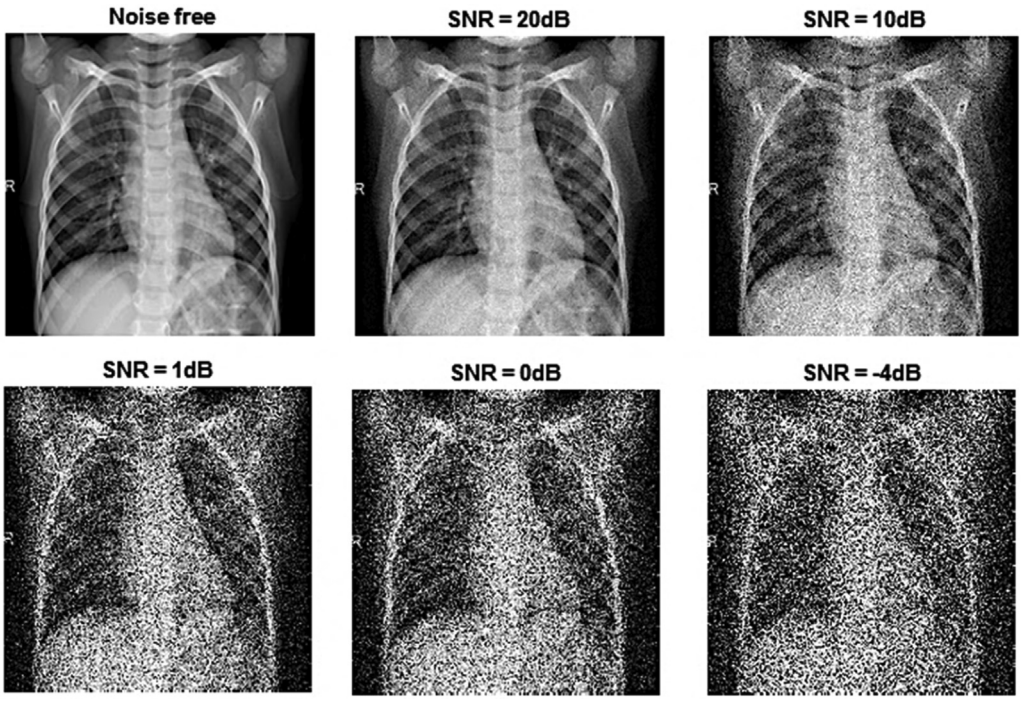

Fig. 17 White Gaussian noise added to chest X-ray images in the different ranges of SNR.

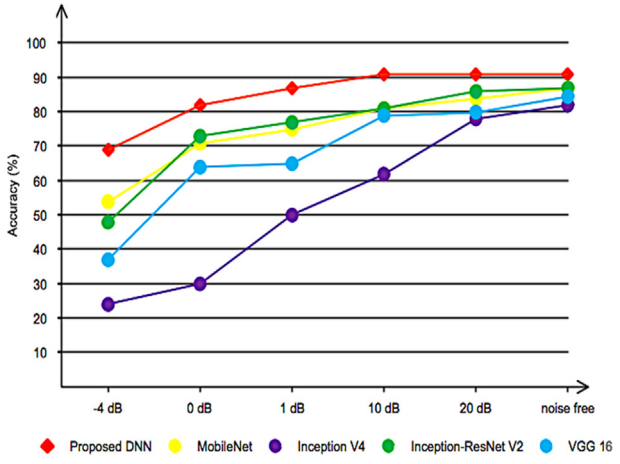

Fig. 18 Comparison of the proposed DNN model robustness with the compared networks in terms of accuracy against additive white Gaussian noise.

is noted that researchers need to use a number of data sets in combination to eliminate the defect; however, the lack of COVID-19 samples is still evident. In this study, GAN networks have been used to address the lack of COVID-19 samples; these networks have recently been used extensively in the field of machine learning and are highly reliable. In the proposed architecture, we also used a modified deep pre-trained network in combination with LSTM networks. The modified pre-trained deep network consisted of two components, including the base and the head which only the head section has been trained from the beginning. Also, as seen from the results section, LSTM networks combined with pre-trained networks have reduced oscillation, increased speed and convergence, and increased the accuracy of the algorithm. In addition, the proposed model works in accordance with the end-to-end learning principle and does not use handcrafted features. As a result, an efficient, fast, and reliable model has been built and promising results have been achieved. Of course, it should not be forgotten that our proposed model has still been evaluated on the scale of several small COVID-19 databases. However, this is not a cause for concern, as we anticipate that, given the nature of the proposed deep network, only training time will increase as the size of the database increases.

6. Conclusion

In this work, an automatic method for classifying pneumonia (including COVID-19) using chest X-ray images based on the proposed DNN was presented. The chest X-ray images were used in the proposed method to separate 2–4 classes into 7 specific and functional scenarios according to healthy, viral, bacterial, and COVID-19 groups. We have achieved an accuracy of more than 90% in all scenarios except one, which is very promising compared to recent research. We also compared our proposed DNN with other deep transfer learning networks (Including Inception-ResNet V2, Inception V4, VGG16, and MobileNet) that have recently been used in pneumonia studies and we achieved very promising results. Furthermore, the classification accuracy of the proposed DNN is considerably robust to the measurement noise in a wide range of SNR. Due to the good performance of the proposed algorithm, it can be used as a smart computer assistant in the field of medicine for rapid diagnosis of pneumonia types (including COVID-19). It is also expected that the use of the suggested automatic method will reduce medical costs, reduce the incidence of nurses and doctors to the COVID-19 during swab sampling, and reduce future mortality in the future.

Table 9 Comparison of the proposed network performance with recent studies.

Methods	Dataset	# of classes	Acc (%)	Se (%)	Sp (%)
Khalifa et al. [19]	Private	2	99	–	–
Huaiguang et al. [11]	Private	2	97	–	–
Chuchan et al. [20]	Public	3	96.39	–	–
Stephen et al. [21]	Public	2	95	–	–
Liang et al. [22]	Public	2	90	–	–
Noor et al. [23]	Public	3	98.97	89.39	99.75
Brunese et al. [24]	Public	2	96	96	98
Loannis et al. [16]	Public	2	93.48	92.85	98.75
Ardakani et al. [25]	Private	2	99.02	98.04	100
Jaiswal et al. [26]	Public	2	96.25	9629	96.21
Ucar et al. [54]	Public	3	98.26	99.13	–
Narin et al. [15]	Public	2	98	–	–
Proposed DNN Model	Public	4 class / 7scenarios	99.5	100	99.02

Declaration of Competing Interest

The authors declare that they have no known competing financial interests or personal relationships that could have appeared to influence the work reported in this paper.

Acknowledgements

This work was supported by Research and Innovation Management Center (PPPI) and Faculty of Engineering, Universiti Malaysia Sabah (UMS) under VOT (TBP0002).

References

[1] L. Yan et al, Prediction of criticality in patients with severe Covid-19 infection using three clinical features: a machine learning-based prognostic model with clinical data in Wuhan, medRxiv (2020).
[2] K. Roosa et al, Real-time forecasts of the COVID-19 epidemic in China from February 5th to February 24th, 2020, Infect. Dis. Modell. 5 (2020) 256–263.
[3] S.B. Stoecklin et al, First cases of coronavirus disease 2019 (COVID-19) in France: surveillance, investigations and control measures, January 2020, Eurosurveillance 25 (6) (2020) 2000094.
[4] V.M. Corman, D. Muth, D. Niemeyer, C. Drosten, Hosts and sources of endemic human coronaviruses, Advances in Virus Research, vol. 100, Elsevier, 2018, pp. 163–188.
[5] C. Huang et al, Clinical features of patients infected with 2019 novel coronavirus in Wuhan, China, The Lancet 395 (10223) (2020) 497–506.
[6] V. Corman, T. Bleicker, S. Brünink, C. Drosten, M. Zambon, Diagnostic detection of 2019-nCoV by real-time RT-PCR, 17, World Health Organization, 2020.
[7] G. Yan et al, Covert COVID-19 and false-positive dengue serology in Singapore, Lancet. Infect. Dis (2020).
[8] H.X. Bai et al, Performance of radiologists in differentiating COVID-19 from viral pneumonia on chest CT, Radiology (2020) 200823.
[9] A. Esposito et al, Why is chest CT important for early diagnosis of COVID-19? Prevalence matters, medRxiv (2020).
[10] T. Ai et al, Correlation of chest CT and RT-PCR testing in coronavirus disease 2019 (COVID-19) in China: a report of 1014 cases, Radiology (2020) 200642.
[11] H. Wu, P. Xie, H. Zhang, D. Li, M. Cheng, Predict pneumonia with chest X-ray images based on convolutional deep neural learning networks, J. Intell. Fuzzy Syst. 1–15 (2020), https://doi.org/10.3233/jifs-191438.
[12] Z. Zhang, P. Cui, W. Zhu, Deep learning on graphs: a survey, IEEE Trans. Knowl. Data Eng. (2020).
[13] F. Shan, et al., Lung infection quantification of covid-19 in ct images with deep learning, arXiv preprint arXiv:2003.04655, 2020.
[14] X. Xu, et al., Deep learning system to screen coronavirus disease 2019 pneumonia, arXiv preprint arXiv:2002.09334, 2020.
[15] A. Narin, C. Kaya, Z. Pamuk, Automatic detection of coronavirus disease (covid-19) using x-ray images and deep convolutional neural networks, arXiv preprint arXiv:2003.10849, 2020.
[16] I.D. Apostolopoulos, T.A. Mpesiana, Covid-19: automatic detection from x-ray images utilizing transfer learning with convolutional neural networks, Phys. Eng. Sci. Med. (2020) 1.
[17] I. Apostolopoulos, S. Aznaouridis, M. Tzani, Extracting possibly representative COVID-19 Biomarkers from X-Ray images with Deep Learning approach and image data related to Pulmonary Diseases, arXiv preprint arXiv:2004.00338, 2020.
[18] P.K. Sethy, S.K. Behera, Detection of coronavirus disease (covid-19) based on deep features, Preprints 2020030300 (2020) 2020.
[19] N.E.M. Khalifa, M.H.N. Taha, A.E. Hassanien, S. Elghamrawy, Detection of Coronavirus (COVID-19) Associated pneumonia based on generative adversarial networks and a fine-tuned deep transfer learning model using chest X-ray dataset, arXiv preprint arXiv:2004.01184, 2020.
[20] V. Chouhan et al, A novel transfer learning based approach for pneumonia detection in chest X-ray images, Appl. Sci. 10 (2) (2020) 559.
[21] O. Stephen, M. Sain, U.J. Maduh, D.-U. Jeong, An efficient deep learning approach to pneumonia classification in healthcare, J. Healthcare Eng. 2019 (2019).
[22] G. Liang, L. Zheng, A transfer learning method with deep residual network for pediatric pneumonia diagnosis, Comput. Methods Prog. Biomed. (2019) 104964.
[23] Majid Nour, Zafer Cömert, Kemal Polat, A Novel Medical Diagnosis model for COVID-19 infection detection based on Deep Features and Bayesian Optimization, Appl. Soft Comput. 106580 (2020).
[24] Luca Brunese et al, Explainable deep learning for pulmonary disease and coronavirus COVID-19 detection from X-rays, Comput. Methods Prog. Biomed. 196 (2020) 105608.
[25] I.D. Apostolopoulos, T.A. Mpesiana, Covid-19: automatic detection from x-ray images utilizing transfer learning with convolutional neural networks, Phys. Eng. Sci. Med (2020) 1.

[26] L. Wang, Z.Q. Lin, A. Wong, Covid-net: a tailored deep convolutional neural network design for detection of covid-19 cases from chest x-ray images, Sci. Rep. 10 (1) (2020) 1–12.
[27] K.F. Haque, F.F. Haque, L. Gandy, A. Abdelgawad, Automatic detection of COVID-19 from chest X-ray images with convolutional neural networks, in: 2020 International Conference on Computing, Electronics & Communications Engineering (iCCECE), IEEE, 2020, pp. 125–130.
[28] Ali Abbasian Ardakani et al, Application of deep learning technique to manage COVID-19 in routine clinical practice using CT images: results of 10 convolutional neural networks, Comput. Biol. Med. (2020) 103795.
[29] Aayush Jaiswal et al, Classification of the COVID-19 infected patients using DenseNet201 based deep transfer learning, J. Biomol. Struct. Dyn. (2020) 1–8.
[30] Michael J. Horry et al, COVID-19 detection through transfer learning using multimodal imaging data, IEEE Access 8 (2020) 149808–149824.
[31] https://www.kaggle.com/paultimothymooney/chest-xray-pneumonia.
[32] https://www.kaggle.com/andrewmvd/convid19-x-rays.
[33] https://towardsdatascience.com/detecting-covid-19-induced-pneumonia-from-chest-x-rays-with-transfer-learning-an-implementation-311484e6afc1.
[34] https://www.kaggle.com/tawsifurrahman/covid19-radiography-database.
[35] https://github.com/ieee8023/covid-chestxray-dataset.
[36] https://www.pyimagesearch.com/2020/03/16/detecting-covid-19-in-x-ray-images-with-keras-tensorflow-and-deep-learning/.
[37] Z. Mousavi, M.M. Ettefagh, M.H. Sadeghi, S.N. Razavi, Developing deep neural network for damage detection of beam-like structures using dynamic response based on FE model and real healthy state, Appl. Acoust. 168 (2020) 107402.
[38] S. Sheykhivand, Z. Mousavi, T.Y. Rezaii, A. Farzamnia, Recognizing emotions evoked by music using CNN-LSTM networks on EEG signals, IEEE Access 8 (2020) 139332–139345.
[39] Z. Mousavi, S. Varahram, M.M. Ettefagh, M.H. Sadeghi, S.N. Razavi, Deep neural networks–based damage detection using vibration signals of finite element model and real intact state: an evaluation via a lab-scale offshore jacket structure, Struct. Health Monit. (2020), 1475921720932614.
[40] Z. Mousavi, T.Y. Rezaii, S. Sheykhivand, A. Farzamnia, S. Razavi, Deep convolutional neural network for classification of sleep stages from single-channel EEG signals, J. Neurosci. Methods 324 (2019) 108312.
[41] S. Sheykhivand, T.Y. Rezaii, Z. Mousavi, A. Delpak, A. Farzamnia, Automatic identification of epileptic seizures from EEG signals using sparse representation-based classification, IEEE Access 8 (2020) 138834–138845.
[42] S. Sheykhivand, T.Y. Rezaii, Z. Mousavi, S. Meshgini, Automatic stage scoring of single-channel sleep EEG using CEEMD of genetic algorithm and neural network (2018).
[43] S. Hochreiter, J. Schmidhuber, Long short-term memory, Neural Comput. 9 (8) (1997) 1735–1780.
[44] O. Wichrowska, et al., Learned optimizers that scale and generalize, in: Proceedings of the 34th International Conference on Machine Learning-Volume 70, 2017: JMLR. org, pp. 3751–3760.
[45] S. Sheykhivand, T.Y. Rezaii, A. Farzamnia, M. Vazifehkhahi, Sleep stage scoring of single-channel EEG signal based on RUSBoost classifier, in: 2018 IEEE International Conference on Artificial Intelligence in Engineering and Technology (IICAIET), 2018, IEEE, pp. 1–6.
[46] S. Sheykhivand, T.Y. Rezaii, A.N. Saatlo, N. Romooz, Comparison between different methods of feature extraction in BCI systems based on SSVEP, Int. J. Ind. Math. 9 (4) (2017) 341–347.
[47] I. Goodfellow, et al., Generative adversarial nets, in: Advances in neural information processing systems, 2014, pp. 2672–2680.
[48] D.A. Schmidt, C. Shi, R.A. Berry, M.L. Honig, W. Utschick, Minimum mean squared error interference alignment, in 2009 Conference Record of the Forty-Third Asilomar Conference on Signals, Systems and Computers, 2009, IEEE, pp. 1106–1110.
[49] Y. Bengio, Rmsprop and equilibrated adaptive learning rates for nonconvex optimization, corr abs/1502.04390, 2015.
[50] C. Szegedy, S. Ioffe, V. Vanhoucke, A.A. Alemi, Inception-v4, inception-resnet and the impact of residual connections on learning, in: Thirty-first AAAI conference on artificial intelligence, 2017.
[51] Y. Li, H. Huang, Q. Xie, L. Yao, Q. Chen, Research on a surface defect detection algorithm based on MobileNet-SSD, Appl. Sci. 8 (9) (2018) 1678.
[52] H. Qassim, A. Verma, D. Feinzimer, Compressed residual-VGG16 CNN model for big data places image recognition, in: 2018 IEEE 8th Annual Computing and Communication Workshop and Conference (CCWC), 2018, IEEE, pp. 169–175.
[53] F. Baldassarre, D.G. Morín, L. Rodés-Guirao, Deep koalarization: Image colorization using cnns and inception-resnet-v2, arXiv preprint arXiv:1712.03400, 2017.
[54] F. Ucar, D. Korkmaz, COVIDiagnosis-Net: Deep Bayes-SqueezeNet based diagnosis of the coronavirus disease 2019 (COVID-19) from X-ray images, Med. Hypotheses 140 (2020), https://doi.org/10.1016/j.mehy. 2020.109761 109761.